Electrochimica Acta 167 (2015) 268–277

Contents lists available at ScienceDirect

Electrochimica Acta

journal homepage: www.elsevier.com/locate/electacta

# A Step Potential Electrochemical Spectroscopy Analysis of Electrochemical Capacitor Electrode Performance

Madeleine F. Dupont, Scott W. Donne *

*Discipline of Chemistry, University of Newcastle, Callaghan, NSW 2308, Australia*

ARTICLE INFO

*Article history:*
Received 8 January 2015
Received in revised form 2 March 2015
Accepted 18 March 2015
Available online 19 March 2015

*Keywords:*
Step potential electrochemical spectroscopy
SPECS
activated carbon
chronoamperometry

ABSTRACT

Step potential electrochemical spectroscopy (SPECS) has been developed as an electrochemical method for application to electrochemical capacitors, in this case for an activated carbon electrode in 0.5 M $H_2SO_4$. The method involves the application of a sequence of small potential steps over the potential window used by the electrode under study, followed by a relatively long rest time after each potential step. Modelling of the SPECS data has been used to extract the contributions made by electrical double layer charge storage and diffusional (redox) processes to the total electrode performance. Outcomes from the application of this approach highlight the dominant charge storage mechanisms at both high and low cycle rates, as well as allow differentiation of 'capacitor-like' or 'battery-like' electrode behaviour. The SPECS data has also been analysed so as to enable calculation of voltammograms at different scan rates for the electrode system. Finally, electrode performance data has also been presented and discussed.


## 1. Introduction

### 1.1. Electrochemical energy storage

The reliable and sustainable production of energy is a critical issue for present and future society. Current fossil fuel based energy production is neither sustainable nor environmentally conscious, while the current crop of renewable energy sources are neither of sufficient scale or cost effective to be taken up broadly by society. As such, significant advances are required in these areas to ensure an energy secure future. In particular, two issues related to renewable energy production and utilization that are of key significance are efficiency and intermittency, both of which can be improved through the use of electrochemical energy storage technologies. Many examples exist in both the popular and scientific literature to demonstrate these advantages [1–5].

Electrochemical energy storage and conversion technologies cover a broad spectrum of devices, including those based on electrolytic and electrochemical capacitors, battery systems and fuel cells [6]. Within each of these categories there are also numerous chemistries, each of which have their own performance characteristics. Often a Ragone diagram (gravimetric or volumetric energy density versus power density) is used to assess device performance; however, these are not the only system properties that are of importance [1,2]. Other characteristics such as cyclability, cost effectiveness, safety and environmental concerns can all play a part in dictating the applicability of a device [1]. In this work our focus is on electrochemical capacitors, which are typified by high power densities, low energy densities, and excellent cyclability [7].

### 1.2. Electrochemical capacitors

The majority of commercial electrochemical capacitors are symmetrical devices based on identical high surface area and porosity activated carbon electrodes immersed in either an aqueous or non-aqueous electrolyte [1]. Energy storage in these devices is via charge separation at the electrode-electrolyte interface; i.e., in the electrified double layer [1]. Research directions for these materials typically focus on novel and optimized carbon material structures and morphologies, and their interface with electrolytes, that ultimately maximize the amount of charge that can be stored at the interface. Activated carbon materials such as these provides 100-200 F/g, with an energy density of 1-2 Wh/kg, power densities up to $10^4$ W/kg, with minimal performance fade for over $10^5$ cycles [1,7–10].

The relatively low energy density of electrochemical capacitors is at the present time a significant impediment to their widespread

* Corresponding author. Tel.: +61 2 4921 5477.
*E-mail address:* scott.donne@newcastle.edu.au (S.W. Donne).

http://dx.doi.org/10.1016/j.electacta.2015.03.137
0013-4686/

applicability. Ultimately the cost per Wh is too high for commercial uptake [1]. Strategies that have been proposed and used to improve this performance characteristic include using alternative electrolytes that enable a larger potential window, and/or using electrode materials that store charge via pseudo-capacitance, which is charge storage through the use of redox reactions at the electrode surface [2]. Materials that have been shown to exhibit pseudo-capacitance include various forms of carbon [11], conducting polymers (such as polypyrrole or polythiophene) [12,13], and metal oxides (such as ruthenium dioxide and manganese dioxide) [14,15]. In each of these cases charge is stored as a result of a facile, reversible redox (faradaic) process for the electrode material at the electrode-electrolyte interface. The energy that can be stored in the three-dimensional structure of the electrode material is higher than that stored at the two-dimensional electrode-electrolyte interface. One question that has arisen regarding the study of this class of materials is related to the relative fraction of charge stored as pseudo-capacitance versus charge stored in the double layer at the electrode-electrolyte interface.

### 1.3. Electrochemical characterization

The ultimate test of how a particular material performs as an electrochemical capacitor electrode is via electrochemical characterization, either in a half-cell (three-electrode) configuration, to focus specifically on the individual electrode material, or in a full cell, as would be used commercially. Certainly many electrochemical methods exist for characterizing materials; however, in the case of electrochemical capacitors cyclic voltammetry (CV) and constant current charge-discharge (CC) cycling are by far the most common. Electrochemical impedance spectroscopy (EIS) is also used, but certainly not as frequently as CV or CC cycling. Ultimately the CV and CC methods provide the user with performance data; i.e., specific capacitance (F/g) as a function of cycling rate, and perhaps some electrode characteristics; e.g., equivalent series resistance (ESR), but rarely is any quantitative mechanistic information provided.

EIS can be used to provide much more quantitative performance and fundamental information about the electrode or system, such as ESR, charge transfer resistance, double layer capacitance, diffusional characteristics, time constant, and reactive power, etc. [16]; however, this analysis is very dependent on the equivalent circuit chosen for modelling, and is also confined to just one potential within the window of the electrochemical capacitor. Furthermore, the application of EIS to two-electrode cells is potentially confounding since is not clear which electrode is causing the cell response.

### 1.4. This work

In this work we have developed and applied step potential electrochemical spectroscopy (SPECS) to the study of electrochemical capacitor electrodes. This method has previously been used to examine the diffusion characteristics of battery cathode materials, particularly with a focus on examining the quasi-equilibrium discharge and charge characteristics, as well as the kinetics of diffusion through the active material structure as a function of applied potential and state of charge [17–20]. More recently, the SPECS method used in this work has been applied to manganese dioxide electrodes and successfully differentiated between the charge storage contribution from faradaic and non-faradaic processes [21]. Here we will use SPECS to differentiate the charge storage mechanisms used in electrochemical capacitor electrodes, as well as a means of examining the rate performance of an electrode material.

## 2. Experimental

### 2.1. Electrode materials and electrolytes

The activated carbon used in this work was prepared in a two stage process. The first stage involved the pyrolysis of coconut husks at 500 °C under a nitrogen atmosphere for 3 h. After cooling the resultant char was milled in a zirconia mill to produce a material with a mean particle size of ~20 μm. In the second stage, activation of the char was carried out with the addition of a small volume of concentrated $H_3PO_4$, with the resultant suspension again pyrolyzed at 700 °C for 1 h under a nitrogen atmosphere.

Electrodes made from the activated carbon were examined in a 0.5 M $H_2SO_4$ electrolyte prepared by dilution of 98% $H_2SO_4$ (98%; Merck) with Milli-Q ultra-pure water (resistivity > 18.2 MΩ.cm).

### 2.2. Surface area and porosity analysis

The surface area and porosity of the activated carbon sample was determined using a Micrometrics ASAP2020 Gas Adsorption and Porosity Analyzer. Samples were pre-treated by degassing under vacuum at 300○ C for 12 hours to remove surface water. A $N_2$ adsorption isotherm (at 77 K) was then measured on each sample covering the partial pressure ($P/P_o$) range $10^{-7}$–1. The specific surface area was then determined using the linearized BET isotherm, while sample porosity was determined using the DFT Plus V2.0 software package from Micromeritics.

### 2.3. Electrode casting

A mixture of the solid electrode components was made by lightly grinding together an 80:10:10 mixture of the activated carbon, carbon black (Cabot Vulcan XC72R; conductive agent), and poly(vinylidenedifluoride) (PVdF; binder) using a ceramic mortar and pestle (~5 min.). This mixture was then made into an ink by adding N-methylpyrrolidone (NMP, 99%) in a ratio of 20:1 solvent to solid (by weight). The ink was stirred for 30 minutes until evenly dispersed.

The working and counter electrodes were cast by dropping 50 μL (mass loading ~0.008 g/cm$^2$ active material) and 100 μL (0.023 g/cm$^2$) of the ink, respectively, onto clean gold-coated stainless steel substrates. The gold-coated stainless steel substrates were prepared by first polishing with 1200 grit emery before being washed thoroughly with Milli-Q water, and wiped dry with a lint free tissue. Gold was then sputter coated onto the stainless steel substrate. The counter electrode had a greater mass than the working electrode to ensure that any limitations of the system were a result of the working electrode. The electrodes were then dried in air at 60 °C for at least 8 hours.

### 2.4. Electrochemical cell construction

The electrochemical cell used was based on a Swagelok 13 mm diameter perfluoroalkoxy alkane (PFA) T-junction. The coated working and counter electrodes were inserted loosely from opposite ends into the cell, initially leaving the third perpendicular port open. The two stainless steel electrodes were then pressed together at 1.7 MPa using a hydraulic press to ensure good cell conductivity, before the electrodes were secured (screwed) into place. The cell was then removed from the press, filled with electrolyte, sealed and left to equilibrate for ~12 h. After equilibration, the reference electrode (saturated calomel electrode; SCE; Radiometer Analytical) was inserted into the perpendicular port of the Swagelok cell and sealed in place with Parafilm. Unless otherwise stated, all potentials stated are with respect to the SCE.

### 2.5. Electrochemical protocol

All electrochemical experiments were conducted using an Iviumstat Multichannel Potentiostat controlled by Iviumstat software. The working electrode was initially pre-treated using cyclic voltammetry. Cycling was conducted between +0.3 and -0.5 V vs SCE using a scan rate of 20 mV/s for 1000 cycles. This was carried out to establish reversible cycling behaviour.

The first stage of the step potential electrochemical spectroscopy experiment was to allow the working electrode to equilibrate at the upper potential limit for 5 min. After this rest period a potential step of -25 mV was applied to working electrode for 300 s to allow for the electrode to equilibrate. During this time the current flow was measured as a function of time. This step process was repeated until the working electrode potential had reached the minimum potential of its electrochemical stability window (-0.5 V). The potential step process was then reversed by stepping in +25 mV increments, again with a 300 s rest time after each step, until the maximum potential was reached (+0.3 V). Under these circumstances the electrode has completed one entire discharge/charge cycle.

## 3. Results and discussion

### 3.1. Surface area and porosity

Gas adsorption analysis of the activated carbon material was conducted to determine the surface area and porosity of the material. The total surface area of the material was calculated to be 1888 $m^2/g$ using the linearized BET isotherm, while Fig. 1 shows the cumulative and incremental pore volume for the material. This data shows that the material has a large proportion of micropores, particularly those with diameter $<10$ Å.

### 3.2. Cyclic voltammetry of the activated carbon electrode

Prior to conducting the SPECS experiment the activated carbon electrode was cycled in 0.5 M $H_2SO_4$ for 1000 cycles at 20 mV/s, between +0.3 V and -0.5 V, to establish stable cycling behaviour. Fig. 2 shows selected voltammograms from the 1000 cycles carried out. The data indicates that the electrode has the expected behaviour of an electrical double layer capacitor; i.e., a 'box-like' voltammogram. The only notable exception is the cathodic current which was essentially constant throughout the potential window, except at low potentials where there is a slight increase due to reduction reactions on the carbon surface potentially involving hydrogen ad-atom formation [22,23]. The cathodic current in this low potential region was significant during the first few cycles, but decayed steadily to achieve a lower steady state current for the remainder of the cycling period.

The specific capacitance of this electrode was calculated by integrating the current (i; A/g) with respect to time (t; s), giving a value for the charge passed (Q; C/g) for the cathodic and anodic scans. This was then converted to a specific capacitance (C; F/g); i.e.,

$$Q = \int_0^t i\,dt \text{ and } C = \frac{Q}{V} \quad (1)$$

where V is the potential window employed (V). All reported values for gravimetric capacitance are with respect to the mass of active material (activated carbon) in the electrode. The specific capacitance for this electrode is shown inset in Fig. 2. The first cathodic half cycle shows the highest specific capacitance, which is consistent with the significant, irreversible reduction reaction at low potentials. Subsequent to this the specific capacitance decays to reach a steady state value of ~130 F/g for the remaining cycles. The charge efficiency (ratio of anodic to cathodic charge) was 0.995 after 1000 cycles.

### 3.3. Step potential electrochemical spectroscopy data

The SPECS experiment was designed so that the electrochemical capacitor electrode could be discharged and charged throughout its potential window via a series of small potential steps, with sufficient rest time between steps to allow for the electrode to reach quasi-equilibrium. Using this equilibration time effectively allows for a very slow scan of the potential window to be carried out; i.e., 25 mV/5 min or 0.083 mV/s. Such a

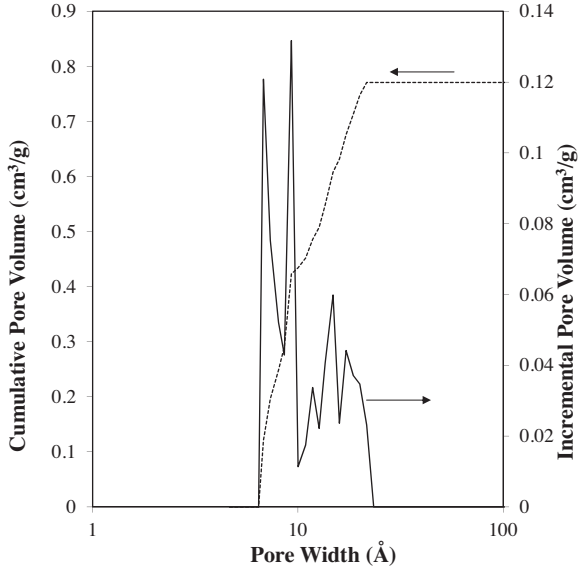


**Fig. 1.** Cumulative and incremental pore volume as a function of pore width (Å) for the activated carbon used in this work.

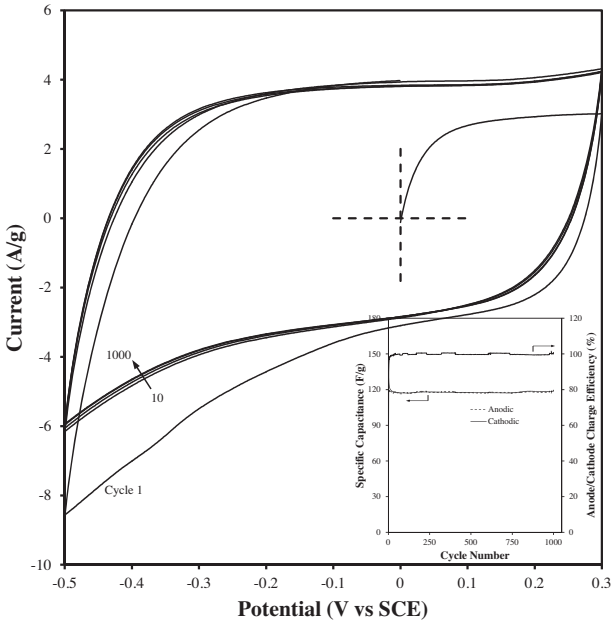


**Fig. 2.** Selected cyclic voltammograms on the activated carbon electrode in 0.5 M $H_2SO_4$. Scan rate: 20 mV/s. Inset: Specific capacitance and charge efficiency as a function of cycle number.

slow scan rate enables the maximum charge storage capabilities of the electrode to be accessed, with the overall resulting current able to be then analyzed for the effects of double layer charge storage, diffusion, redox reactions and electrochemical kinetic limitations.

A typical i-t response for a +25 mV potential step applied to the activated carbon electrode under study is shown in Fig. 3. Just like in a standard chronoamperometry experiment [24], the current spikes to a maximum value, after which it decays quickly to essentially zero by the end of the time period. For an electrical double layer capacitor this current profile is the result of charging the double layer at the electrode-electrolyte interface. However, for a pseudo-capacitive electrode the current flow is due to a combination of double layer charge storage and redox reactions at the electrode surface, including the kinetics of these processes, as well as diffusion of the electro-active species, either through the electrolyte to the electrode surface, or through the solid state into the structure of the electrode material [1] When the current drops to zero or a constant value, an equilibrium state is implied.

When this process is repeated over the full potential window the result is as shown in Fig. 4. The current response exhibits a series of current maxima corresponding to each 25 mV step (either positive or negative), followed by a current decay. It is evident that not all of the potential steps result in a current response similar to that in Fig. 3, but nevertheless the shape of the data is basically the same. Some potential steps result in a much slower current decay, while others have a substantial equilibrium current.

### 3.4. Contributions to the overall current

At any electrified interface there are a number of basic processes that can occur. Charge carriers approaching the electrode surface from the electrolyte can either undergo a redox process at the interface or contribute to charge build-up in the electrical double layer [24]. Along with these basic actions it is also common to observe diffusional processes [1], either to or from the electrode surface, which may be heterogeneous, rough or porous. With this in mind, the intent here is to further characterize the SPECS data from the activated carbon electrode by fitting each individual current response to various mathematical models to evaluate the contributions of such electrode processes to the total charge stored.

Charge storage in activated carbon is most often attributed to electrical double layer storage. Double layer charging is a fast, facile process and as such, decays very quickly after the potential step is applied. The current response ($i_C$; A/g) for a double layer capacitor upon the application of a potential ($E_S$; V) is given by [24]:

$$i_C = \frac{E_S}{R_S} \exp\left(-\frac{t}{R_S C_C}\right) \quad (2)$$

where $R_S$ is the series resistance ($\Omega$/g) attributable to the resistance of the electrodes, electrolyte and material in the electrochemical cell, $C_C$ is the double layer capacitance (F/g), and t is the time after the potential step (s).

Faradaic redox processes typically involve consumption of an electro-active species at the electrode surface, in which case mass transport has to occur to replenish the species just consumed. Mass transport under such circumstances is by diffusion in response to the concentration gradient emanating from the electrode surface. The most common approach to modelling this type of process is through the use of the Cottrell equation for semi-infinite planar diffusion [24], in which case:

$$i_D \propto t^{-1/2} \quad (3)$$

Here the decay in current is much slower than charging of the electrical double layer. It should be noted here that these diffusional processes can occur on both the geometric and porous surfaces of the activated carbon particles.

What should be also noted from Fig. 4 is that the current response for many of the potential steps does not decay to zero, even after the full equilibration time period. Both Eqs. (2) and (3) do not allow for the establishment of a non-zero steady state current, and so an additional constant current term is also necessary. The origin of this residual current ($i_R$; A/g) is likely to do with a sustained, ongoing redox reaction occurring at the electrode surface that is kinetically limited; i.e., a redox process in which

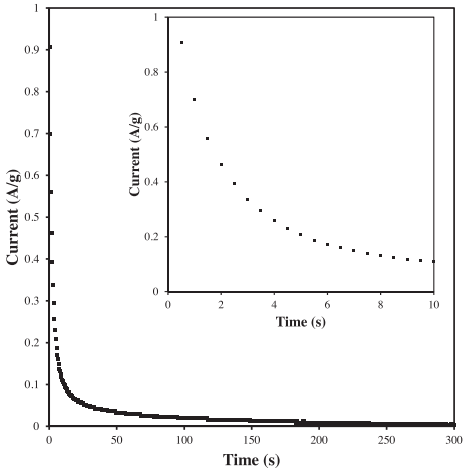


**Fig. 3.** Typical i-t response for a +25 mV potential step on the activated carbon electrode in 0.5 M $H_2SO_4$. Step to -0.400 V vs SCE. Inset: Expanded plot of the current change during the early stages of the step.

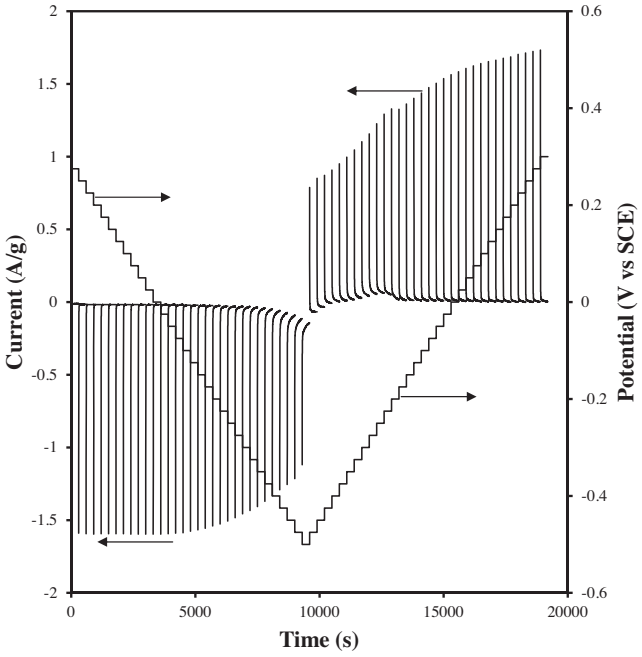


**Fig. 4.** Complete step potential electrochemical spectroscopy (SPECS) data set for the activated carbon electrode in 0.5 M $H_2SO_4$. The SPECS experiment involves a 25 mV potential step followed by a 300 s rest period, sequenced over the full potential window from 0.3 V to -0.5 V vs SCE to generate a full cycle.

mass transport is not limiting, but rather the act of charge transfer is limiting. It is likely that this process also involves the solvent (i.e., a reactant in large excess) given the magnitude of the residual current at certain potentials.

Therefore, the total current ($i_T$; A/g) flowing during each potential step in the SPECS experiment was modelled using the combined expression:

$$i_T = i_C + i_D + i_R = \frac{E_S}{R_S} \exp\left(-\frac{t}{R_S C_C}\right) + \frac{B}{t^{1/2}} + F \quad (4)$$

where $R_S$, $C_C$, B and F are the fitting parameters, evaluated by linear least squares regression. Fig. 5 shows an example of the data fitting. In terms of the goodness of fit between Eq. (4) and the experimental data the correlation coefficient was always greater than 0.99, indicating an excellent fit at all potentials during the cycle.

### 3.5. Separating Faradaic and double layer charge storage

Using the fitting parameters determined in the previous section, together with the expressions to determine the total charge and hence the specific capacitance (Eq. (1)), each experimental i-t data set can be broken down into its components, which can then be converted into a specific capacitance. This breakdown is shown in Fig. 6.

#### 3.5.1. Series resistance

The series resistance ($R_S$) within the cell takes into consideration the resistance of all aspects of the cell design including interfacial resistances between the electrode and substrate, the electrode itself, as well as the electrolyte. The value of $R_S$ is a key determinant in the overall power output (P; Wh/kg) of the electrochemical capacitor device [1,25], with lower $R_S$ values corresponding to higher power outputs; i.e., $P \propto 1/R$. Starting with the cathodic scan, $R_S$ was ~13 mΩ/g of activated carbon at +0.3 V, increasing slowly up to ~20 mΩ/g at a potential of -0.275 V. As the SPECS experiment progressed to lower potentials $R_S$ increased dramatically, reaching ~87 mΩ/g at the end of the cathodic section of the SPECS experiment (-0.5 V). While the overall value of $R_S$ is still not large, the systematic increase in its value is of concern. Comparing $R_S$ with the full SPECS dataset in Fig. 4 it is apparent that the increase in $R_S$ corresponds with an increase in the faradaic electrode processes, particularly those that are sufficiently slow that the electrode does not reach a zero current by the end of the potential step. As mentioned previously, this sustained current may be due to the reaction of the activated carbon with the water solvent at these low potentials, possibly leading to the formation of hydrogen ad-atoms on the surface. The reduction reaction could potentially be the formation of hydrogen by electrochemical decomposition of the electrolyte. In the 0.5 M $H_2SO_4$ electrolyte used here the expected reduction potential of hydrogen is -0.241 V vs SCE which is within the cycling window used here. The reduction of hydrogen ions to form hydrogen is a two-step mechanism involving initially hydrogen ad-atom formation on the electrode surface; i.e.,

$$H^+(aq) + e^- \rightarrow H_{ad} \quad (5)$$

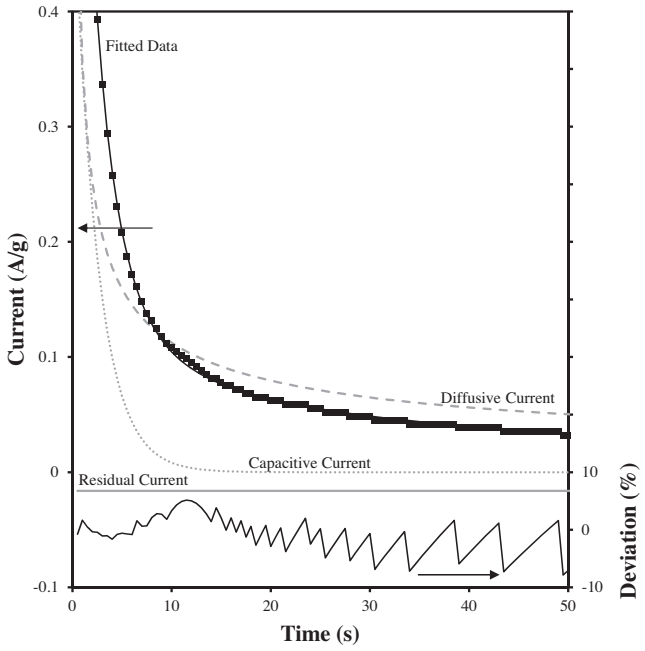


**Fig. 5.** Fitting of the i-t data from an individual SPECS step showing the contributions from capacitive, diffusive and residual current, as well as the deviation between the experimental and predicted data.

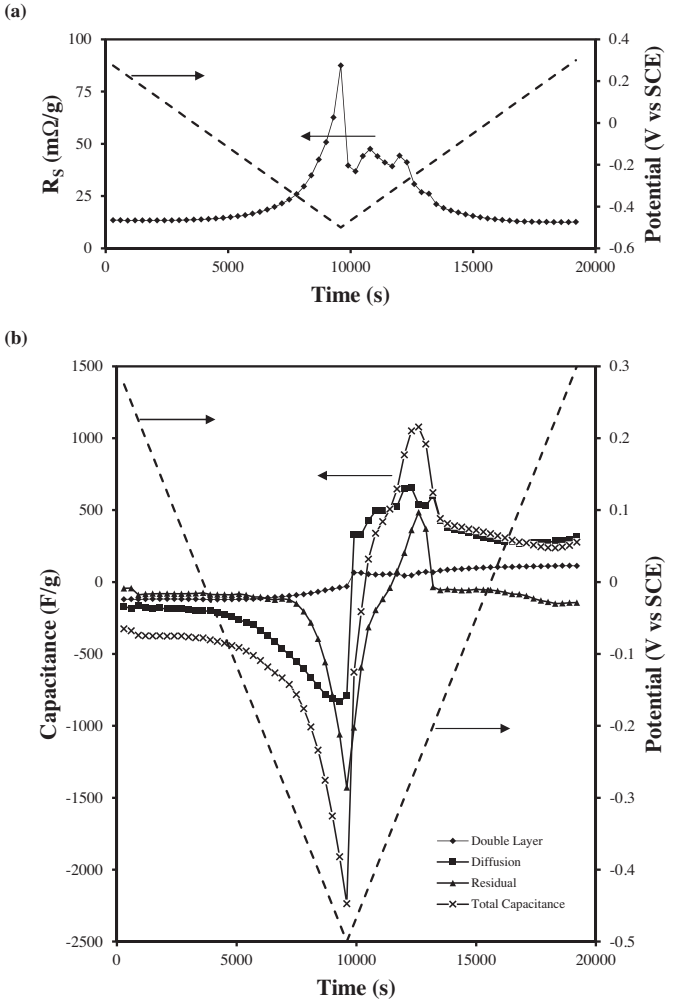


**Fig. 6.** Variation in (a) the series resistance ($R_S$), and (b) the contributions to the total capacitance for the activated carbon electrode in 0.5 M $H_2SO_4$ as a function of applied potential. Each point was determined from the SPECS experiment which involved a 25 mV potential step followed by a 300 s relaxation period.

This is then followed by hydrogen gas formation via either of the following reactions, the choice of which is dependent on the substrate; i.e.,

$$2H_{ad} \rightarrow H_2(g) \quad (6a)$$

$$H^+(aq) + H_{ad} + e^- \rightarrow H_2(g) \quad (6b)$$

The formation of hydrogen ad-atoms on the electrode surface would increase the resistance between the electrode and the electrolyte, explaining the increased series resistance at cathodic potentials. The adsorption of hydrogen onto activated carbon has previously been reported [11]. The presence of these species may lead to an increased resistance between particles and hence an overall increase in electrode resistance. During the anodic section of the SPECS experiment $R_S$ decreases as the potential increases, although at low potentials the decrease in $R_S$ is not as systematic as it was during the cathodic section. In this instance this may be due to the electrochemical re-oxidation of the hydrogen ad-atoms on the activated carbon surface. Ultimately, $R_S$ returns to its initial value after a full cycle; however, the apparent presence of redox processes in this potential window dramatically influences the resistance of the electrode.

*3.5.2. Double layer capacitance ($C_C$)*

The double layer capacitance from this activated carbon electrode in 0.5 M $H_2SO_4$ appears to be a minor contributor to the total capacitance. Starting at ~120 F/g at +0.3 V, $C_C$ remains essentially constant during the cathodic sweep until a potential of ~-0.325 V, where the value of $C_C$ begins to decline until it reaches ~30 F/g at -0.5 V. This decrease in double layer capacitance coincides with an increase in cathodic current, as seen in Fig. 2, and also an increase in the residual current flowing, as seen in Fig. 4. When the direction of the SPECS experiment was reversed to be anodic the value of $C_C$ was in the range 50-70 F/g until a potential of -0.175 V was reached, after which $C_C$ increased gradually to retain its starting value of ~120 F/g at +0.3 V. As with the cathodic sweep, low value of $C_C$ were noted to occur when high residual currents were noted in the anodic series of potential steps, as shown in Fig. 4.

*3.5.3. Capacitance from diffusional processes ($C_D$)*

The capacitance associated with diffusional processes was found to be the major contributor to the total electrode capacitance. At the start of the SPECS experiment a capacitance of ~170 F/g was measured at +0.3 V, essentially increasing exponentially to ~780 F/g at -0.5 V. This dramatic increase in specific capacitance during the cathodic part of the SPECS experiment was of course due to the increasing prevalence of the diffusional current over the full timeframe of the applied potential step. As seen in Fig. 5, the decay in diffusional current is much slower than the capacitive current, and as a result significantly more charge can be transferred during the potential step. The origin of these diffusional processes lies with the redox reactions that the activated carbon can undergo in the aqueous acidic medium. At low potentials, below -0.125 V, where the contributions from diffusional processes increase dramatically, significant reduction reactions are occurring on the activated carbon surface. These may be related to the re-reduction of oxygen-rich functional groups on the carbon surface, such as hydroxyl, ketone, aldehyde or carboxylic acid groups, or potentially the formation of hydrogen ad-atoms on the activated carbon surface, as a step in the mechanism of hydrogen evolution. In either case, the substantial increase in charge, and hence specific capacitance, of the activated carbon electrode at these low potentials must be associated with a redox reaction between the electrolyte and the activated carbon. Upon reversal of the SPECS direction, $C_D$ exhibits some features in the potential range -0.5 V to -0.15 V that are again associated with redox reactions on the activated carbon surface, in this case oxidation processes. These are likely due to oxidation of the previously formed hydrogen ad-atoms on the activated carbon surface, or oxidation of the carbon surface to form oxygenated functional groups. From the data in Fig.1 the balance between cathodic and anodic capacitance in this potential region is not balanced, suggesting that the efficiency of hydrogen ad-atom re-oxidation is poor, or alternatively that some hydrogen evolution may have occurred at low potentials, leading to hydrogen that is lost to the electrolyte and is hence not recoverable. At the highest potentials (+0.3 V) the capacitance related to diffusion processes does increase slightly, potentially due to oxidation of the carbon surface.

*3.5.4. Residual capacitance ($C_R$)*

The residual capacitance parameter indicates that a sustained reaction is occurring, one which does not decay to zero over the equilibration period, such as the decomposition of the electrolyte. From Fig. 6 it is apparent that the residual capacitance is associated closely with the diffusional capacitance. $C_R$ becomes a significant contributor to the total capacitance at low potentials in both the cathodic and anodic SPECS half cycles; i.e., in the potential range -0.375 V to -0.5 V in the cathodic half cycle, where $C_R$ grows from ~120 F/g to ~630 F/g, and in the range -0.5 V to -0.2 V in the anodic half cycle. It is very interesting to note that the residual capacitance is essentially all cathodic, except in the potential window -0.325 V to -0.2 V during the anodic half cycle. This is potentially indicative of the ongoing reduction reactions occurring in the full potential window covered.

Another aspect that needs to be considered in relation to the residual capacitance is mass transport in pores. As covered in the previous section, faradaic processes occurring at the activated carbon surface dominate the total charge storage of the electrode. Over the relatively long timeframe taken during each potential step in the SPECS experiment, particularly at low potentials, there is a sustained ongoing redox reaction, that as mentioned above, involves consumption of the electrolyte. Given that the activated carbon is very porous, this means that the electrolyte must move into the pores to replenish what has been consumed as a result of the redox reactions. Depending on the size of the pores and their surface chemistry, this rate of mass transport may vary considerably. Therefore, in addition to the redox reactions occurring, the slow transport of electrolyte to the reaction sites on the surface through pores may extend beyond the 300 s used in this case.

*3.5.5. Total capacitance ($C_T$)*

What will be noted about the total capacitance associated with this activated carbon electrode is that it is very large compared to what is conventionally extracted from an activated carbon electrode in 0.5 M $H_2SO_4$. As can be seen in Fig. 2 when cycled at 20 mV/s, the activated carbon electrode exhibits only ~130 F/g. Interestingly, this is highly comparable to the double layer capacitance contribution extracted from the SPECS data, despite the much smaller potential window used for each step in the SPECS experiment. Of course the difference between the data in Figs. 2 and 6 is that the SPECS experiment was conducted at a rate of 0.083 mV/s, which is much slower than that collected in Fig. 2 (20 mV/s). What is clear, therefore, is that the slower SPECS scan rate allows for the much slower diffusional (faradaic) and residual processes to emerge and begin to contribute to the electrode capacitance, so much so that at the cycling rate of the SPECS experiment, they dominate the contributions to the overall capacitance.

### 3.6. Predicting electrochemical capacitor rate performance

The SPECS experiment at first glance would seem to be completely different to a cyclic voltammetry experiment. However, most modern digital potentiostats carry out linear sweep voltammetry or cyclic voltammetry experiments using a series of small potential steps combined with a short residence time at that potential. For example, a 0.02 mV/s scan rate corresponds to a 1 mV potential step every 50 s. The choice of potential step and residence time is determined by the user; however, most often a small as possible potential step is employed. In the present SPECS experiment the equivalent scan rate is 0.083 mV/s (25 mV/300 s).

Another user controlled variable during a linear or cyclic voltammetry experiment using a digital instrument is how the current is recorded during the small potential step. Most often the default is to measure current over the entire duration of the potential step, and then record an average current at that particular potential. Given this description of current measurements, there are of course considerable similarities with the present SPECS experiment, the only difference being of course that the final step of averaging the current has not been carried out. Therefore, for each potential step average current values ($i_{AV}$) have been calculated as a function of time after the onset of the potential step; i.e.,

$$i_{AV} = \frac{1}{n}\sum_{n=1}^{t_n} i_n \tag{7}$$

where n is a counter corresponding to each individual current and time data point; i.e., ($i_n$, $t_n$). The time used for the summation in Eq. (7) can then be used to determine the scan rate (v; V/s) for the corresponding voltammetry experiment; i.e,

$$v = \frac{E_S}{t} \tag{8}$$

where $E_S$ is the magnitude of the potential step (0.025 V in this case), as in Eq. (1), and t is the time after application of the potential step (s). An example of this calculation for this electrode system is shown in Fig. 7. With a decaying current after the application of the potential step, it is apparent from Eqs. (7) and (8) that short times correspond to fast scan rates and higher currents, whereas longer times lead to slower scan rates.

Now using the average current at a fixed time after each potential step, such as shown in Fig. 7, a voltammogram can be constructed that uses the corresponding average current for each potential step. Such a series of voltammograms are shown in Fig. 8. What is first apparent from these voltammograms is that the measured current is higher for the faster scan rates, which is of course an expected result. Secondly, and perhaps what is more significant, is that as the scan rate decreases, features in the voltammogram begin to emerge, in this case the peaks present in the anodic scan between -0.5 V and -0.2 V. As was established above, these processes were associated with redox processes, which now with slower scan rates become much more apparent in the voltammogram. To explore this further, the same approach that was used to calculate the voltammograms in Fig. 8 from the experimental data, was applied to the capacitive, diffusional and residual components that were extracted from each step in the SPECS experiment. The result is shown in Fig. 9(a) at 50 mV/s and Fig. 9(b) for 0.1 mV/s. At the higher cycle rate the voltammogram derived from the experimental SPECS data appears as you would expect for a double layer capacitor material; i.e., a 'box-like' voltammogram over the full potential window. This is largely a consequence of the double layer contributions which dominate for most of the potential window, except for at low potentials where there is a comparable contribution from the diffusional characteristics of the electrode. Across the full potential window the residual current contributions are minimal. At low scan rates, however, the situation is very different. The bulk of the voltammorgam is dominated by diffusional (redox) processes, with very little coming from double layer charge storage. At low potentials even the residual current contributes more to the total current than double layer charge storage. Furthermore, features in the voltammogram again become apparent that were not able to be observed at higher scan rates. The implication here is that for a pseudo-capacitive electrode systems such as the activated carbon electrode in 0.5 M $H_2SO_4$ used here, there is a transition from what is traditionally

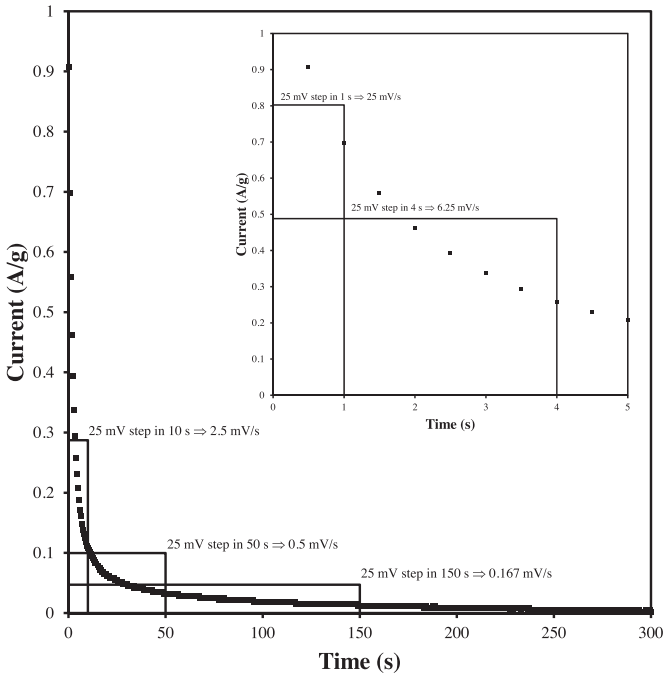


**Fig. 7.** Examples of the calculated average current as a function of time after the potential step in a SPECS experiment.

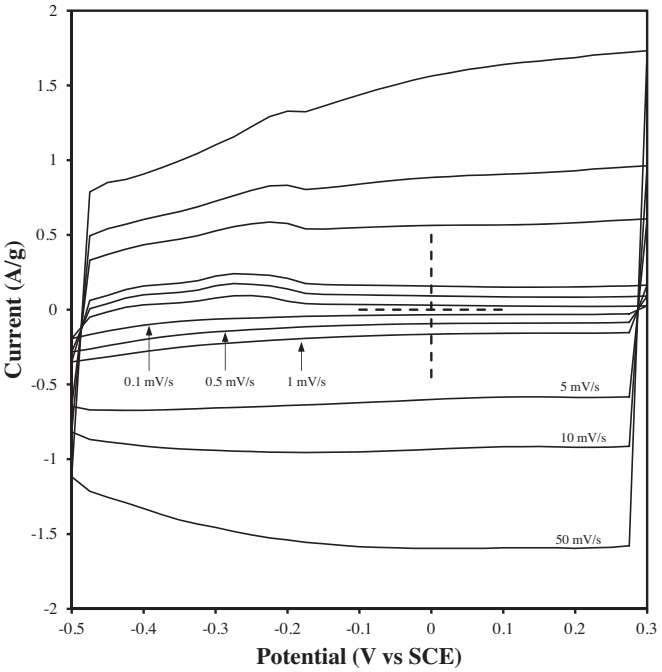


**Fig. 8.** Calculated voltammograms from the SPECS data.

classified as an electrical double layer capacitor electrode system at high rates where diffusional or redox processes are minimal because their rates of reaction or mass transport are too slow, to a redox active or pseudo-capacitive electrode material in which the electrical double layer contributes only a minor amount to the total capacitance, which is otherwise dominated by the contributions from redox processes.

Before proceeding further it is appropriate at this stage to comment on the assumptions made in the conversion of SPECS data into voltametric data. Recall that the key to transforming the SPECS data to voltametric data is calculating the average current for a specified time after the potential step. While the current data up to and including the specified time is used for determining the average current, the data after this time is not considered. This infers that the electrode processes after to the time necessary for the average current calculation do not have an effect on latter processes caused by subsequent potential steps.

Since we have developed an approach to calculating voltammograms from the SPECS data, we can also now more conventionally determine the specific capacitance of the electrode as a function of the scan rate. Using the scan rate to convert the working electrode potential to a time basis, Eq. (1) can be used to calculate the specific capacitance not only for the experimentally derived voltammetry data, but also for the double layer, diffusion and residual current contributions. The outcome from this is shown in Fig. 10, where the calculated specific capacitance is shown as a function of scan rate. What the data in this figure shows is that firstly the overall rate performance continues to increase as the scan rate decreases. The implication here is that the activated carbon is reacting with the electrolyte, continuing to extract more charge from the electrode as the scan rate is decreased, and hence increasing the specific capacitance. From the perspective of a real device this is clearly not sustainable as the electrolyte is being consumed and will ultimately lead to cell failure.

At high scan rates the specific capacitance is dominated by contributions from the double layer capacitance, as was inferred from Fig. 9. However, as the scan rate was slowed down the contributions from double layer charge storage reach a plateau, indicating that the double layer has reached a saturation limit. This value is specific to the combination of activated carbon electrode and 0.5 M $H_2SO_4$ electrolyte used in this situation, and as such can be used a comparative diagnostic tool for differentiating for example activated carbon materials in the same electrolyte.

At high scan rates it is equally as important to note that the residual and diffusional contributions to the total specific capacitance are also quite low. The implications of this observation are that the kinetics of these processes are not sufficiently fast to be able to contribute at high rates. However, as the scan rate was decreased the contributions made by both diffusional and residual contributions increased dramatically. The fact that these contributions increase with a decreasing scan rate is again indicative of their much slower reaction kinetics. Secondly, the fact that these

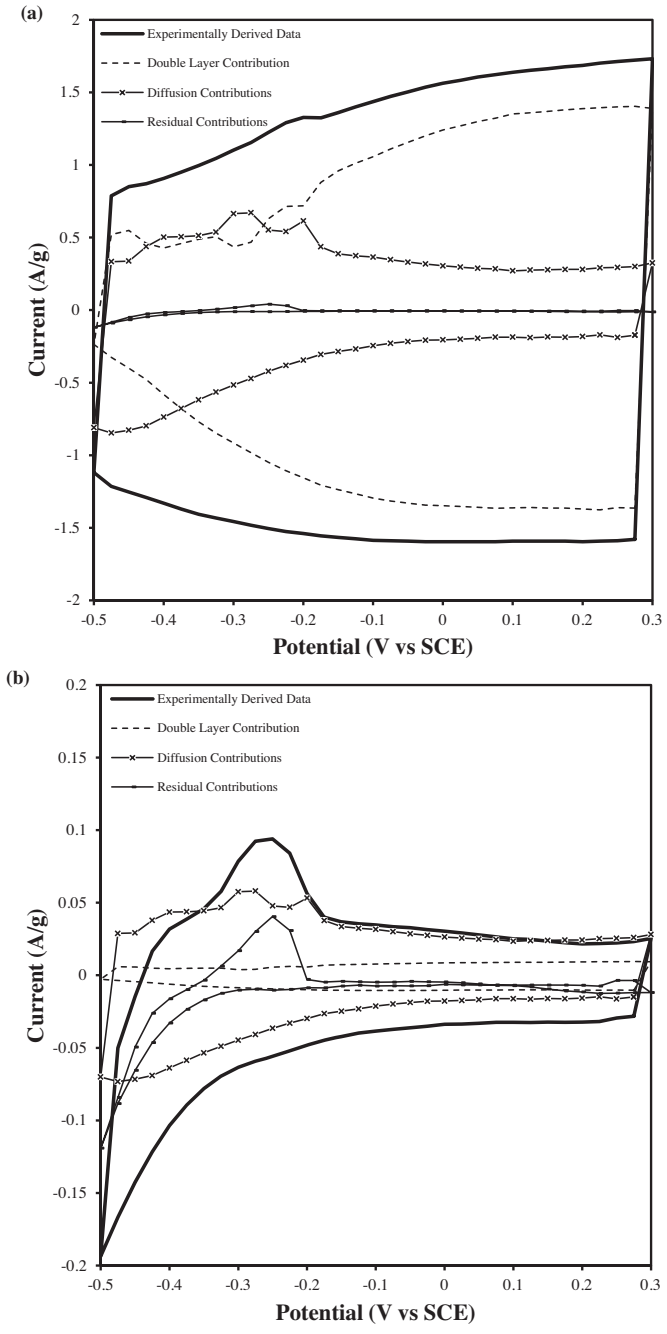


**Fig. 9.** Breakdown of contributions to the total voltametric data for (a) 50 mV/s and (b) 0.1 mV/s.

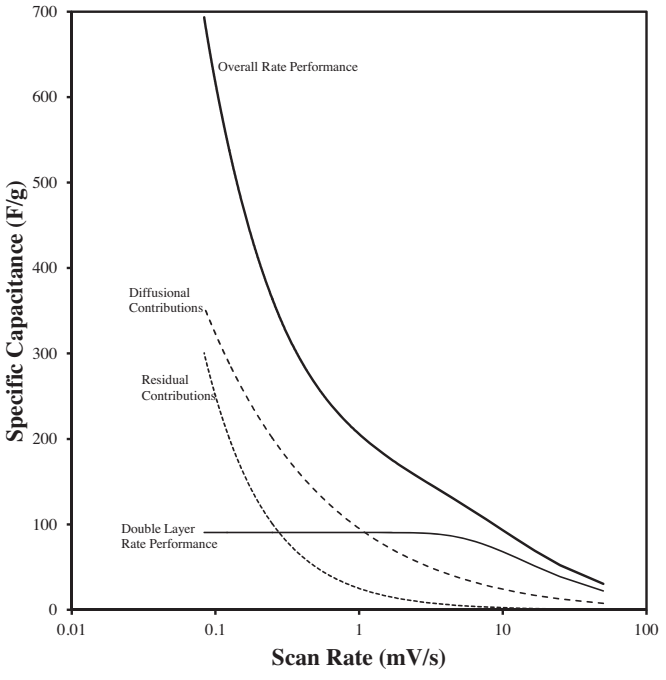


**Fig. 10.** Calculated specific capacitance for each of the contributions to overall performance shown as a function of scan rate.

contributions are not bounded, unlike the double layer capacitance, also implies that the corresponding electrochemical processes involve reactions between the activated carbon and the electrolyte; i.e., those species present in high concentration. As mentioned above, these types of redox processes are not sustainable in an electrochemical device that has a finite reserve of electrolyte.

### 3.7. Specific energy and power

Using the specific capacitance data shown in Fig. 10 we were then able to calculate the specific energy and power for the activated carbon electrode under study. At this time it is important to point out that the specific energy and power values calculated here are for an individual electrode, not a full cell, which is of course the desired set of circumstances. Nevertheless, the application of SPECS to a full cell could be used to evaluate overall performance, albeit with the response being determined by the combination of both individual electrodes. In the case reported here the focus has been on individual electrode behaviour, through the use of a three-electrode arrangement, and as such the resultant specific power and energy are for an individual electrode. As such, the specific energy (E; Wh/kg) of the electrode was determined using

$$E = \frac{1}{2}CV^2 \tag{9}$$

where C is the specific capacitance modified to be in units of Ah/kg, and V is the potential window employed (V). Specific power (P; W/kg) was determined using the expression:

$$P = \frac{E}{t} \tag{10}$$

where E is the specific energy (Wh/kg), and t is the duration of the discharge half cycle in the voltammogram (h). The calculation of specific energy and power was carried out on all contributions to the electrode performance, and is shown in Fig. 11 (Ragone diagram). The significance of the data in this figure is that it provides a breakdown of the contributions to the total electrode performance, a feature of the electrode that has not been described previously in the literature. Also shown in the figure are lines connecting the data points calculated for the same scan rates, highlighting both higher and lower cycle rates. Firstly, the overall performance is comparable with that reported previously for an electrochemical capacitor electrode [7,25–27]. What is perhaps the most significant difference is the increased specific energy at low scan rates, arising primarily from diffusional and residual processes within the electrode. As mentioned previously, these processes are related to redox reactions between the activated carbon and electrolyte that are neither sustainable nor wanted in an electrochemical capacitor device. At high scan rates double layer charge storage contributes the most to the overall performance, particularly in terms of the specific power output from the electrode. This again emphasizes the differences in kinetics between charge storage processes used by the electrode, with fast charge storage in the electrical double layer being kinetically faster than the kinetics of the redox processes at the electrode surface, and the mass transport of electro-active species either to or from the electrode surface. Furthermore, the breakdown of contributions in Fig. 11 demonstrates that redox processes; i.e., pseudo-capacitance, can indeed be used to enhance the specific energy of an electrochemical capacitor electrode, although in the case reported here, this is detrimental to the overall electrode stability and viability.

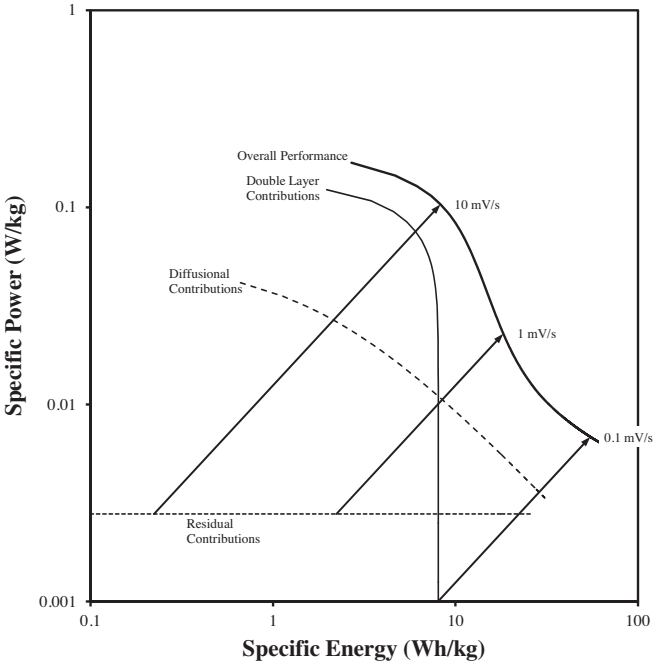


**Fig. 11.** Breakdown of the overall electrode performance, as assessed by a Ragone diagram, in terms of the double layer, diffusional and residual contributions.

## 4. Summary and conclusions

Step potential electrochemical spectroscopy (SPECS) has been developed to characterize the behaviour of electrochemical capacitor electrodes. Conventional methods of electrochemical analysis such as cyclic voltammetry and constant current charge-discharge cycling provide only limited data on the electrode under study. However, SPECS has been shown to more fully characterize the electrochemical response of an electrochemical capacitor electrode. The main outcomes from the present study include:

(i) Refinement of the SPECS method: This method involves applying a relatively small potential step to the electrode under study followed by a rest period to allow for electrode equilibration. This process is repeated to cover the full potential window of the electrode, both cathodic and anodic half cycles. Modelling of the i-t data resulting from each potential step has been carried out using terms to account for double layer charge storage, diffusional processes associated with redox reactions, and a residual current, which in this case we have ascribed to either slow porous diffusion of electro-active species or a sustained reaction between the activated carbon electrode and the electrolyte.

(ii) The i-t data from each potential step (including the experimental data and the modelled components) across the full potential window was then used to calculate representative voltammograms for the electrode at different scan rates by averaging the current out to specified times after the potential step. The resultant voltammograms highlight the most important contributors to the overall performance at different scan rates, in particular that double layer charge storage dominates at high scan rates, while diffusional processes dominate at lower scan rates. The separation of contributions to the overall result emphasizes the cause of the transition from what is conventionally considered to be a capacitor electrode to a battery electrode; i.e., that the kinetics of charge storage in the electrical double layer are much faster than those of the diffusional redox processes, and as such double layer charge storage dominates at high scan rates, leading to a 'box-like' voltammogram, while at slow scan rates 'battery-like' electrode behaviour is observed as a result of faradaic contributions dominating the electrode behaviour.

(iii) With the calculation of voltammograms, the specific rate performance of the electrode under study was determined as a function of scan rate. The overall performance was broken down into its individual contributions, again highlighting the dominance of kinetically facile double layer charge storage at high cycle rates, and the much slower diffusional processes at slow scan rates.

(iv) Specific power and energy were also calculated from the electrode specific capacitance and plotted as a Ragone diagram. It was again shown that these performance characteristics depend on the type of charge storage, whether in the electrical double layer or via faradaic processes.

Overall, SPECS has been shown to be a robust electrochemical method for fully evaluating the electrochemical performance of an electrochemical capacitor electrode. The method emphasizes the contributions to the overall performance, and provides guidance on the stability of electrodes.

## Acknowledgement

MFD acknowledges the University of Newcastle for the provision of a PhD scholarship.

## References

[1] F. Beguin, E. Frackowiak, Supercapacitors Materials, Systems, and Applications, in: M. Lu (Ed.), 1st ed., Wiley-VCH, Weinheim, 2013.
[2] P. Simon, Y. Gogotsi, Materials for electrochemical capacitors, Nature Materials 7 (11) (2008) 845–854.
[3] B.E. Conway, Electrochemical Supercapacitors. Scientific Fundamentals and Technological Applications, Kluwer Academic/Plenum Publishers, New York, 1999.
[4] Electrochemical Energy Storage for Renewable Sources and Grid Balancing., in: P.T. Moseley, J. Garche (Eds.), 1st ed., Elsevier, Amsterdam, 2015.
[5] J. Miller, P. Simon, Electrochemical capacitors for energy management, Science Magazine, 2008, pp. 651–652.
[6] Garche, J., et al., Encyclopedia of Electrochemical Power Sources. ed. J. Garche. 2009, Elsevier: Amsterdam.
[7] Y. Zhang, et al., Progress of electrochemical capacitor electrode materials: A review, International Journal of Hydrogen Energy 34 (11) (2009) 4889–4899.
[8] D. Qu, H. Shi, Studies of activated carbons used in double-layer capacitors, Journal of Power Sources 74 (1) (1998) 99–107.
[9] M. Wang, L.-h, Toyoda, M. Inagaki, Dependence of electric double layer capacitance of activated carbons on the types of pores and their surface areas, New Carbon Materials 23 (2) (2008) 111–115.
[10] Q.-Y. Li, et al., Novel activated carbons as electrode materials for electrochemical capacitors from a series of starch, Solid State Ionics 179 (7–8) (2008) 269–273.
[11] E. Frackowiak, et al., Supercapacitor electrodes from multiwalled carbon nanotubes, Applied Physics Letters 77 (15) (2000) 2421–2423.
[12] B.C. Kim, J.M. Ko, G.G. Wallace, A novel capacitor material based on Nafion-doped polypyrrole, Journal of Power Sources 177 (2008) 665–668.
[13] A. Balducci, et al., Cycling stability of a hybrid activated carbon//poly(3-methylthiophene) supercapacitor with N-butyl-N-methylpyrrolidinium bis (trifluoromethanesulfonyl) imide ionic liquid as electrolyte, Electrochimica Acta 50 (11) (2005) 2233–2237.
[14] P. Kurzweil, et al., CAPACITORS/Electrochemical Metal Oxides Capacitors, in: C. K. Dyer (Ed.), Encyclopedia of Electrochemical Power Sources, Elsevier, Amsterdam, 2009, pp. 665–678.
[15] C.D. Lokhande, D.P. Dubai, O.-S. Joo, Metal Oxide thin film based supercapacitors, Current Applied Physics 11 (3) (2011) 255–270.
[16] M.E. Orazem, B. Tribollet, Electrochemical Impedance Spectroscopy, Wiley, New Jersey, 2008.
[17] A. Cormie, et al., Cycle stability of birnessite manganese dioxide for electrochemical capacitors, Electrochimica Acta 55 (25) (2010) 7470–7478.
[18] M.R. Bailey, S.W. Donne, Electrochemical Impedance Spectroscopy Study into the Effect of Titanium Dioxide Added to the Alkaline Manganese Dioxide Cathode, Journal of the Electrochemical Society 158 (7) (2011) A802–A808.
[19] G.J. Browning, S.W. Donne, Proton diffusion in γ-manganese dioxide, Journal of Applied Electrochemistry 35 (9) (2005) 871–878.
[20] M.F. Dupont, et al., Mass Transport Properties of Manganese Dioxide Phases for Use in Electrochemical Capacitors: Structural Effects on Solid State Diffusion, Journal of the Electrochemical Society 160 (8) (2013) A1219–A1231.
[21] M.F. Dupont, S.W. Donne, Separating the Faradaic and Non-Faradaic Contributions to the Total Capacitance for Different Manganese Dioxide Phases, Journal of the Electrochemical Society 162 (5) (2015) A5096–A5105.
[22] E. Frackowiak, F. Béguin, Electrochemical storage of energy in carbon nanotubes and nanostructured carbons, Carbon 40 (10) (2002) 1775–1787.
[23] K. Jurewicz, E. Frackowiak, F. Béguin, Towards the mechanism of electrochemical hydrogen storage in nanostructured carbon materials, Applied Physics A 78 (7) (2004) 981–987.
[24] A.J. Bard, L.R. Faulkner, Electrochemical Methods: Fundamentals and Applications, 2nd ed., John Wiley & Sons, Inc., New York, 2001.
[25] E. Frackowiak, F. Béguin, Carbon materials for the electrochemical storage of energy in capacitors, Carbon 39 (6) (2001) 937–950.
[26] W. Xing, et al., Superior electric double layer capacitors using ordered mesoporous carbons, Carbon 44 (2) (2006) 216–224.
[27] Y. Zhao, et al., Easy synthesis of ordered meso/macroporous carbon monolith for use as electrode in electrochemical capacitors, Materials Letters 62 (3) (2008) 548–551.